6α-cluster resonance structures in $^{12}C+^{12}C$ system and their decay in α and ^8Be channels

E. T. Mirgule, M. A. Eswaran, Suresh Kumar, D. R. Chakrabarty, V. M. Datar, U. K. Pal, H. H. Oza, and N. L. Ragoowansi
Nuclear Physics Division, Bhabha Atomic Research Centre, Mumbai, 400 085, India

(Received 15 May 1997)

The excitation functions have been measured for the $^{12}C(^{12}C,\alpha)^{20}Ne$ and $^{12}C(^{12}C,^8Be)^{16}O$ reactions leading to the excited states up to 25 MeV in ^{20}Ne and 20 MeV in ^{16}O, respectively, in the beam energy range $E(^{12}C)=48$–72 MeV. The region of excitation investigated was $E_x=38$–50 MeV in ^{24}Mg which is well above the threshold for breakup into six alpha particles. In the ^8Be channel leading to the 6–7 MeV region of ^{16}O, excitation functions were also measured for ^8Be-γ coincidences in $^{12}C(^{12}C,^8Be)^{16}O^*\rightarrow\gamma+^{16}O_{g.s.}$ particularly to distinguish between the otherwise unresolved 6.05 MeV, 0^+ and 6.13 MeV, 3^- states in ^{16}O. It is observed that a cluster of resonances in the excitation region 39–43 MeV in ^{24}Mg decays via α and ^8Be channels predominantly to the particle-hole states in ^{20}Ne and ^{16}O which are members of deformed bands. Another cluster of resonances in the region 44–49 MeV (centered at $E_{c.m.}=32.5$ MeV) decays predominantly to the 20.48 MeV state in ^{20}Ne (which is above the 5α breakup threshold) and to a possible 4α linear chain band in ^{16}O around 18 MeV, indicating their highly deformed nature. This latter cluster structure coincides in energy with the possible 6α linear chain resonance identified in the literature at $E_{c.m.}=32.5$ MeV in the inelastic scattering channels $^{12}C_{7.65,0^+}+^{12}C_{7.65,0^+}$ and $^{12}C_{7.65,0^+}+^{12}C_{9.64,3^-}$. In this excitation energy region intermediate structures in the ^8Be channel are found at $E_{c.m.}=31.5$ and 33.5 MeV decaying to the 6.13 MeV, 3^- state and at $E_{c.m.}=32.5$ MeV decaying to the 6.92/7.13 MeV states of ^{16}O. Similar resonances in the same energy region in inelastic scattering channels $^{12}C_{g.s}+^{12}C_{9.64,3^-}$ and $^{12}C_{g.s.}+^{12}C_{7.65,0^+}$ have also been reported in the literature. It is conjectured from the present measurements that in this region of excitation in ^{24}Mg (44–49 MeV) there are at least two types of states excited in the collision of $^{12}C+^{12}C$. The first type consists of 6α cluster resonances, possibly with large deformation, leading to outgoing channels above the breakup threshold into constituent alpha particles in both the products and the other type leading to outgoing channels below this threshold. [S0556-2813(97)04410-5]

PACS number(s): 25.70.Ef, 21.60.Gx, 25.70.Gh, 27.30.+t

I. INTRODUCTION

There has been considerable interest in recent years in the study of highly deformed alpha particle cluster states in nuclei in the *sd* shell. Particularly, the heavy ion resonance phenomena observed in the elastic and the inelastic scattering of $^{12}C+^{12}C$ were interpreted in terms of highly deformed molecular states in the compound system at high excitation energy above 20 MeV [1]. Extremely deformed alpha particle cluster configurations were also predicted at high excitations in *sd* shell nuclei by structure calculations in the cranked cluster model [2], the deformed shell model [3], and the Hartree-Fock model [4]. The relationship between the heavy ion resonances in $^{12}C+^{12}C$ system and superdeformed states in ^{24}Mg has also been brought out by detailed cluster calculations of Marsh and Rae [2]. The various nuclear models referred to above also predict the existence of highly deformed structures in $A=4n$ light nuclei which resemble a linear chain of alpha particles. The ^8Be ground state has possibly a 2α structure and in ^{12}C the 7.65 MeV, 0_2^+ state is believed to have a highly deformed 3α structure [5]. In ^{16}O there are three levels around 18 MeV decaying predominantly into two ^8Be nuclei. The level spacings of these states with spins 2^+, 4^+, and 6^+ are consistent with those of a band characterized by a large moment of inertia [6]. Wuosmaa *et al.* [7] reported a broad resonance in the $^{12}C+^{12}C$ system at $E_x=46.4$ MeV ($E_{c.m.}=32.5$ MeV) in ^{24}Mg with $J^\pi=(14^+, 16^+)$ which decays into two $^{12}C(0_2^+)$ nuclei, indicating the possibility of its having an alpha linear chain structure. Near this energy other inelastic scattering channels have also been studied [8]. Recently a resonance with $J^\pi=18^+$ has been identified in the inelastic channel $^{12}C_{g.s.}+^{12}C(3^-)$ [9] at $E_{c.m.}=33.5$ MeV. A theoretical explanation of the 6α-chain-like state was reported [10] in terms of the shape eigenstate which is formed coherently from near-degenerate resonances with different spins. In ^{24}Mg this 6α-chain state is predicted by the cluster model [2] at an excitation energy where this resonance is actually observed. The threshold for breakup of ^{24}Mg into 6α particles is at $E_x=28.5$ MeV. Rae and Merchant [11] also reported a schematic coupled channel model of a 6α-chain state in terms of scattering of two lighter α-chain nuclei. They concluded that if the resonance at $E_{c.m.}=32.5$ MeV is to be identified with an aligned 6α-chain state, then it should have large decay widths to specific excited states of ^{16}O and ^8Be. In this context with a view to investigating the region of excitation in ^{24}Mg where highly deformed six-alpha-cluster states are expected, we carried out excitation function measurements in the $^{12}C+^{12}C$ reaction. The outgoing alpha and ^8Be channels leading to several states in ^{20}Ne and ^{16}O, respectively, were measured. The measurements were made in the outgoing channels: (1) $\alpha+^{20}Ne$ at $\theta_{lab}=8°$ and 12°, (2) $^8Be+^{16}O$ at $\theta_{lab}=0°$ and 12°, and (3) $^8Be+^{16}O+\gamma$ at $\theta_{^8Be}=0°$ and θ_γ = 90° and 138° in the energy range $E(^{12}C)=48$–72 MeV ($E_x=38$–50 MeV in ^{24}Mg). Some of the preliminary results of this work were reported earlier [12].

 © 1997 The American Physical Society

II. EXPERIMENTAL DETAILS AND MEASUREMENTS

The excitation functions were measured simultaneously for the $^{12}C(^{12}C,\alpha)^{20}Ne$ and $^{12}C(^{12}C,^{8}Be)^{16}O$ reactions over the range of incident energies of E_{lab}=48–78 MeV in steps of 1 MeV using the momentum-analyzed ^{12}C beam from the BARC-TIFR 14UD Pelletron at Mumbai. The target was a self-supporting natural carbon foil of thickness 40 μg/cm^2 (estimated from the energy loss of 5.486 MeV α particles). The beam was stopped in a Faraday cup and the accumulated charge, measured by a current integrator, was used for normalization in the excitation function measurements.

Two surface barrier ΔE-E detector telescopes were placed at 8° and 12°, respectively, to the beam for particle identification of reaction products in a scattering chamber of 1 m diameter. The telescope at 12°, consisting of ΔE-E detectors of thickness 43 μm and 2 mm, respectively, was placed at a distance of 10.8 cm from the target subtending a solid angle of 8.15 msr (angular acceptance $\pm 2.9°$). The large solid angle of this detector was chosen to enable the detection of ^{8}Be [13], the ground state of which decays into two alpha particles moving in the forward cone in the laboratory. The effective solid angle for $^8Be_{g.s.}$ detection was calculated numerically using a computer program [14]. This was in the range of 15%–30% of the geometric solid angle for the relevant kinetic energies of ^{8}Be. The efficiency for simultaneous detection of two alpha particles in this telescope arising from the decay of the excited states of ^{8}Be is negligible. This telescope enabled the detection of α particles as well as ^{8}Be for the simultaneous measurement of excitation functions for the $^{12}C(^{12}C,\alpha)^{20}Ne$ and $^{12}C(^{12}C,^{8}Be)^{16}O$ reactions. The telescope at 8° consisted of ΔE-E detectors of thickness 46.8 μm and 2 mm, respectively. It was kept at a distance of 15.9 cm from the target, subtending a solid angle of 1.1 msr (angular acceptance $\pm 0.7°$). A tantalum foil of 60 mg/cm^2 thickness was used in front of this detector to stop elastically scattered carbon ions.

Two-dimensional ΔE versus E spectra were recorded in an on-line computer for both the telescopes at each beam energy. In the identification of ^{8}Be from the two-dimensional spectra (in the 12° telescope), an ambiguity could arise from the interference of the ^{7}Li events [15]. However, since the Q value of the reaction $^{12}C(^{12}C,^{7}Li)^{17}F$

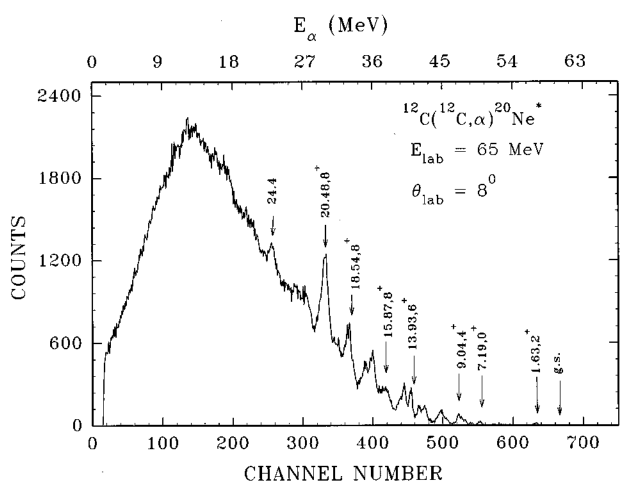

FIG. 1. Measured α spectrum in the ΔE-E detector telescope at θ_{lab}=8° in $^{12}C(^{12}C,\alpha)^{20}Ne^*$ reaction at E_{lab}=65 MeV. Peaks are identified by energy (in MeV) and spins of states in ^{20}Ne. Energies of outgoing α particles, E_α, are shown on the top.

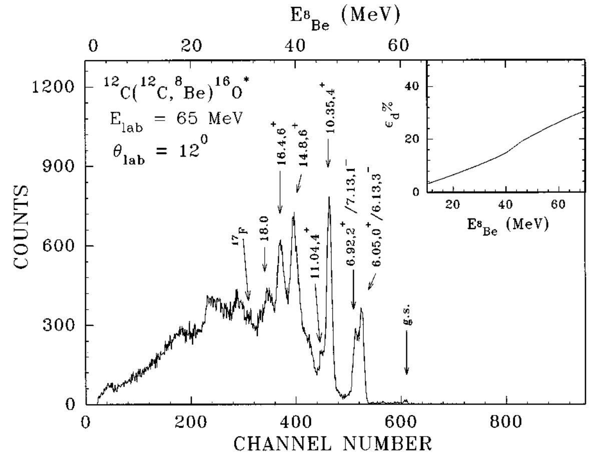

FIG. 2. Measured ^{8}Be spectrum in the ΔE-E detector telescope at θ_{lab}=12° in the $^{12}C(^{12}C,^{8}Be)^{16}O^*$ reaction at E_{lab}=65 MeV. Peaks are identified by energy (in MeV) and spins of states in ^{16}O. Energies of outgoing ^{8}Be particles, $E_{^8Be}$ are also shown on the top. Inset shows the ^{8}Be detection efficiency ϵ_d of the detector as a function of energy of ^{8}Be.

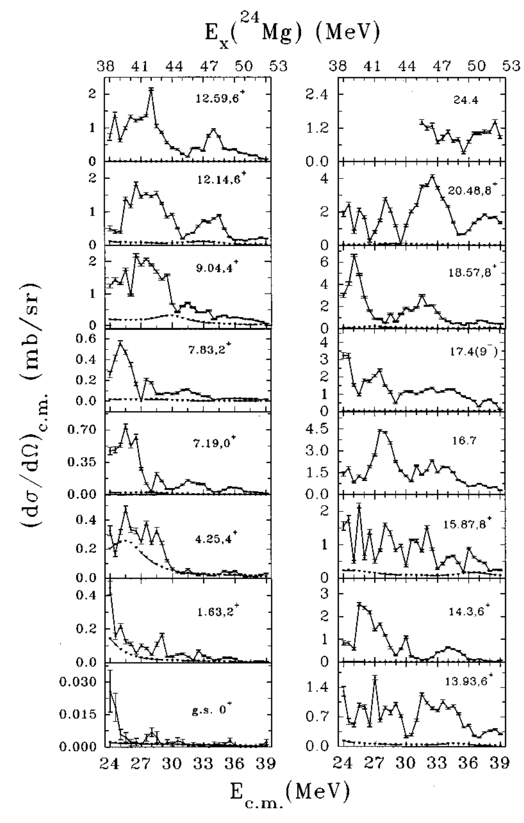

FIG. 3. Excitation functions for the $^{12}C(^{12}C,\alpha)^{20}Ne^*$ reaction at θ_{lab}=8° leading to various states of ^{20}Ne indicated by their energy (in MeV) and spins. The dot-dashed lines show the calculated average cross sections from the statistical (Hauser-Feshbach) model. Calculated cross sections are shown only for those states which are identified to be single states as inferred from the peak widths in the spectrum.

is 16.6 MeV more negative than that of the $^{12}C(^{12}C,^{8}Be)^{16}O$ reaction, the identification was unambiguous up to an excitation energy of ~17 MeV in ^{16}O.

An example of the α-particle spectrum recorded in the ΔE-E telescope at 8° at a beam energy of 65 MeV is shown in Fig. 1. This spectrum was obtained by setting an appropriate two-dimensional gate on the ΔE-E spectrum. The alpha groups leading to various excited states of ^{20}Ne in the $^{12}C(^{12}C,\alpha)^{20}Ne^*$ reaction can be clearly identified as marked in Fig. 1. Above about 9 MeV excitation in ^{20}Ne the α-particle peaks ride on a continuum which increases rapidly with excitation energy. The continuum can arise due to the statistical decay of the compound nucleus, and from the breakup of the projectile or target. In this spectrum the α-particle groups feeding the excited states up to ~ 25 MeV in ^{20}Ne can be identified. The overall width of the peaks is about 250 keV. An example of the ^{8}Be spectrum recorded in the ΔE-E telescope at 12° at a beam energy of 65 MeV is shown in Fig. 2. This was obtained by setting a suitable two-dimensional gate in the ΔE-E spectrum. The ^{8}Be groups leading to various states of ^{16}O in the $^{12}C(^{12}C,^{8}Be)^{16}O^*$ reaction can be clearly identified up to an excitation energy of 18 MeV in ^{16}O as marked in Fig. 2. The continuum in this spectrum has a similar origin to that for alphas mentioned above. The inset in Fig. 2 shows the detection efficiency ϵ_d of the ΔE-E telescope for ^{8}Be detection as a function of the kinematic energy of ^{8}Be particles. The peak areas of the various alpha groups were extracted from the particle spectra, subtracting a smooth background where necessary, at each beam energy to determine the differential cross sections. The excitation functions were determined for 16 and 12 states in ^{20}Ne for the telescopes at 8° and 12°, respectively. Some of the final states, for which excitation functions have been measured, could not be resolved. The excitation functions for the alpha channels are shown in Figs. 3 and 4 for the detectors at 8° and 12°, respectively. Similarly in the case of the $^{12}C(^{12}C,^{8}Be)^{16}O^*$ reaction the excitation functions were deduced for all the peaks marked in Fig. 2. These excitation functions are shown in Fig. 5 for

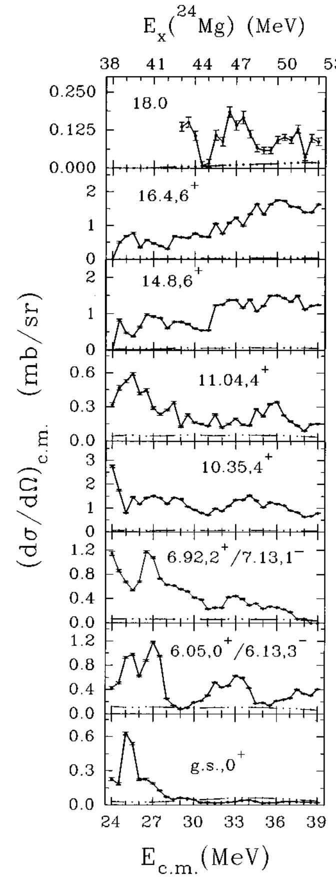

FIG. 5. Excitation functions for the $^{12}C(^{12}C,\ ^{8}Be)^{16}O^*$ reaction at $\theta_{lab} = 12°$ to different states of ^{16}O. The energies and spins of ^{16}O states are also shown. The dot-dashed lines show the stastistical model (Hauser-Feshbach) calculations of the average cross sections.

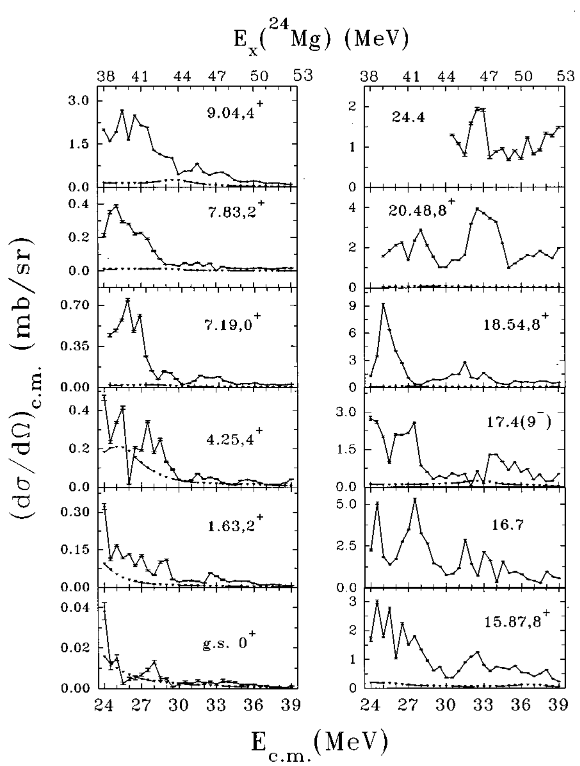

FIG. 4. Excitation functions for the $^{12}C(^{12}C,\alpha)^{20}Ne^*$ reaction at θ_{lab}=12°. Other details are same as in Fig. 3.

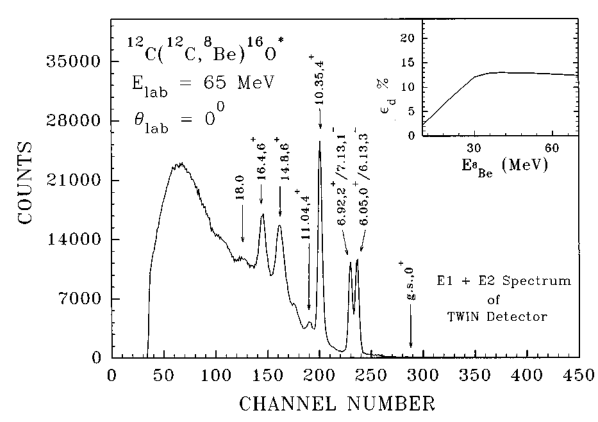

FIG. 6. Measured ^{8}Be spectrum in TWIN detector at $\theta_{lab} = 0°$ in the $^{12}C(^{12}C,\ ^{8}Be)^{16}O^*$ reaction at $E_{lab} = 65$ MeV. Peaks are identified by energy (in MeV) and spins of states in ^{16}O. Inset shows the ^{8}Be detection efficiency ϵ_d of the detector as a function of energy of ^{8}Be.

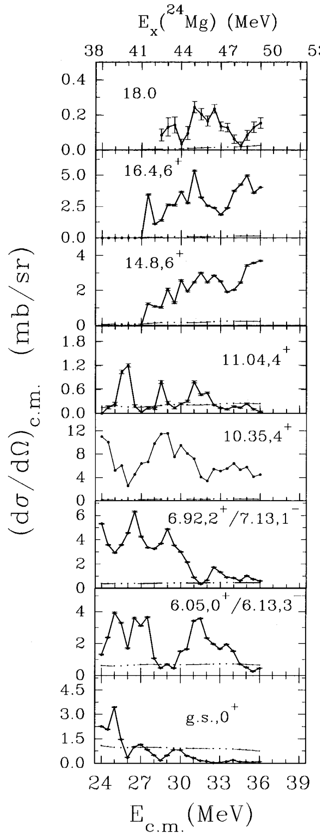

FIG. 7. Excitation functions for the $^{12}C(^{12}C,^{8}Be)^{16}O^*$ reaction at $\theta_{lab}=0°$ to different states of ^{16}O. The energy (in MeV) and spins of ^{16}O states are also shown. The dot-dashed lines show the stastistical model (Hauser-Feshbach) calculations of the average cross sections.

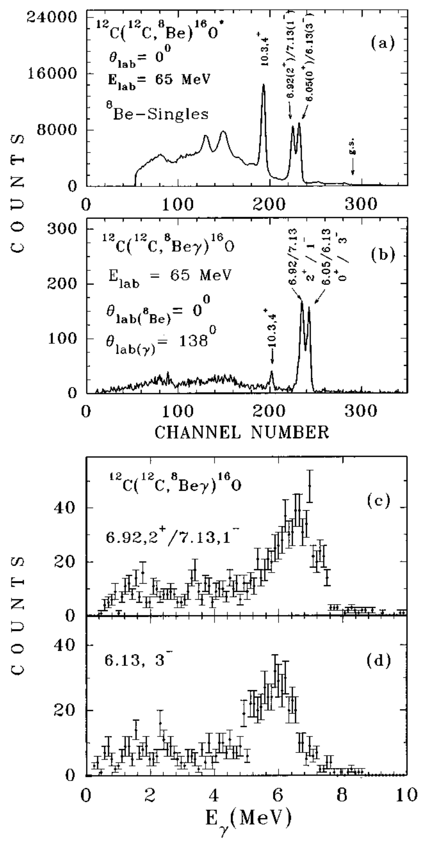

FIG. 8. (a) Measured ^{8}Be spectrum in the ΔE-E detector telescope at $\theta_{lab}=0°$ in the $^{12}C(^{12}C,^{8}Be\gamma)^{16}O^*$ reaction at $E_{lab}=65$ MeV. Peaks are identified by energy (in MeV) and spins of states in ^{16}O. (b) ^{8}Be spectrum in the same detector telescope in coincidence with all γ rays recorded in the BaF_2 detector at $\theta_\gamma= 138°$. (c) Spectrum of γ rays recorded at $\theta_\gamma=138°$ in coincidence with ^{8}Be leading to the 6.92/7.13 MeV states of the ^{16}O and (d) to 6.13 MeV, 3^- state of ^{16}O.

^{8}Be leading to various excited states of ^{16}O.

In order to eliminate any doubt about a possible contamination of the ^{8}Be spectrum by ^{7}Li particles, particularly at the higher excitation energy near 18 MeV in ^{16}O, the excitation function measurements were repeated in a separate experiment. In this experiment the ^{8}Be particles were identified using an α-α coincidence method using a large area split (TWIN) detector at 0°. This silicon surface barrier detector had a diameter of 18 mm and a 1 mm insulating gap along its diameter so that each half could function as an independent detector. The thickness of the depletion layer was $\sim$400 μm. The TWIN detector was placed at 0° to the beam at a distance of 10.8 cm subtending a solid angle of 15.1 msr (angular acceptance $\pm 3.9°$). The effective solid angle for ^{8}Be detection was calculated using a Monte Carlo simulation program. It was in the range of 15%–25% of the geometric solid angle for the energies of ^{8}Be in the present work. The beam was stopped in front of the 0° detector by using a tantalum foil of thickness 60 mg/cm^2. The data were recorded as coincidence two dimensional spectra of $E1$versus $E2$ where $E1$ and $E2$ are the energies of the α particles in the two halves of the detector. In this experiment also the excitation functions were measured in steps of 1 MeV over a beam energy range of E_{lab} = 48–72 MeV. An example of the ^{8}Be spectrum recorded in the TWIN detector is shown in Fig. 6. This spectrum is obtained by setting a software gate in the two-dimensional $E1$ versus $E2$ spectrum

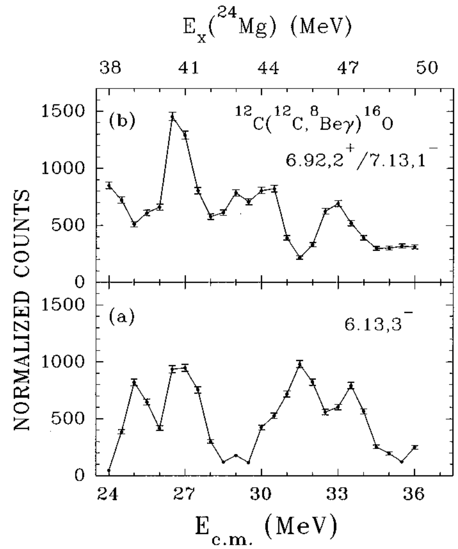

FIG. 9. (a) Excitation function for the $^{12}C(^{12}C,^{8}Be\gamma)^{16}O$ reaction with ^{8}Be leading to (a) 6.13 MeV, 3^- state and (b) 6.92,2^+/7.13,1^- states in ^{16}O. The data of θ_γ = 138° and θ_γ =90° are summed.

to select ^{8}Be events and summing $E1$ and $E2$. The excitation functions obtained from these spectra are shown in Fig. 7.

The excitation functions in the $^{12}C(^{12}C,^{8}Be)^{16}O$ reaction, particularly feeding the 6–7 MeV excitation region of ^{16}O, show resonances in the region of $E_{c.m.}$= 30–35 MeV. In the 6 MeV region of ^{16}O there are two closely spaced states, viz., the 6.05 MeV, 0^{+} four-particle–four-hole $(4p\text{-}4h)$ state and the 6.13 MeV, 3^{-} octupole state. In the excitation function measurements these two states could not be resolved. Hence we have measured the excitation function for ^{8}Be leading to the 6–7 MeV region of ^{16}O in coincidence with high energy γ rays arising from the decay to the ground state. In this experiment a self-supporting natural carbon target of thickness 55 μg/cm^{2} was used. ^{8}Be was detected at 0° using a ΔE-E surface barrier telescope placed inside a small scattering chamber at a distance of 11 cm from the target. The detector telescope consist of ΔE-E detectors of thickness 28 μm and 2 mm, respectively, and subtended a solid angle of 8.25 msr and had an angular acceptance of $\pm 2.9°$. The beam was stopped in front of the detector using a tantalum foil of thickness 60 mg/cm^{2}. γ rays were detected in hexagonal BaF_{2} detectors having face to face distance of 9 cm and thickness of 20 cm. Two such detectors were used outside the scattering chamber at 90° and 138° to the beam and at a distance of 16 cm from the target. The beam current was limited to about 10 particle nA in order to keep the count rates in the γ detectors within reasonable limits. Data were recorded as coincidence events between the ^{8}Be detector and the γ detectors in the list mode on a computer-based data acquisition system. The coincidence excitation function was measured for beam energies of E_{lab}=48–72 MeV in steps of 1 MeV.

The ^{8}Be spectrum recorded in the 0° telescope is shown in Fig. 8(a) for the beam energy of 65 MeV. The list mode data were analyzed by putting various software gates using a computer program and finally reduced to two-dimensional $E1$ versus E_{γ} spectra, where $E1$is the energy of ^{8}Be in 0° detector and E_{γ} is the energy of the γ ray deposited in the BaF_{2} detectors. Figure 8(b) shows the energy spectrum of ^{8}Be in coincidence with all γ rays, i.e., the projection of $E1$ versus E_{γ} spectrum on the $E1$ axis, at 65 MeV for θ_{γ}= 138°. Figure 8(c) shows the γ ray spectrum in coincidence with ^{8}Be feeding the 6.92/7.13 MeV states of ^{16}O while Fig. 8(d) shows the spectrum of γ rays in coincidence with ^{8}Be feeding the 6.13 MeV, 3^{-} state in ^{16}O. For the extraction of coincidence excitation functions events in the full energy peak of the γ-ray spectrum were included. The random coincidences were less than 5% and were subtracted. The coincidence excitation functions (after summing data for θ_{γ}= 90° and 138°) are shown in Figs. 9(a) and 9(b), for 6.13 MeV, 3^{-} and $6.92(2^{+})/7.13(1^{-})$ states of ^{16}O, respectively.

III. ANALYSIS OF DATA

The excitation functions for the $^{12}C(^{12}C,\alpha)^{20}Ne^{*}$ reaction leading to various excited states of ^{20}Ne are shown in Figs. 3 and 4, for θ_{lab}=8° and 12°, respectively. Similar excitation functions for the $^{12}C(^{12}C,^{8}Be)^{16}O^{*}$ reaction at θ_{lab}=12° and 0° are shown in Figs. 5 and 7, respectively. Some of these excitation functions show prominent structures. These structures can be due to the presence of resonances or statistical fluctuations due to overlapping levels. The presence of a correlation between different exit channels for the observed structure in the excitation functions is an important evidence [16,17] for heavy ion resonances as opposed to statistical fluctuations [18]. We first compare, in Sec. III A, the measured cross sections with the Hauser-Feshbach statistical model [19] calculations for both reactions leading to various excited states. In Sec. III B, we shall discuss the statistical versus nonstatistical features of the observed structures. In Sec. III C, the analysis of the data taken in coincidence with gamma rays will be presented.

A. Hauser-Feshbach statistical model calculations

The Hauser-Feshbach statistical model calculation, which is based on the statistical decay probabilities into all available open channels, reflects the average compound nuclear cross sections. In this case the differential cross section for decay into a particular exit channel is given by [20]

$$\frac{d\sigma_{\alpha\alpha'}}{d\Omega}=\sum_{L}\frac{1}{4}\left(\frac{\lambda}{2\pi}\right)^{2}\sum_{J}\frac{1}{(2I+1)(2i+1)}\frac{\left[\sum_{s,l}T_{l}(\alpha)\right]^{J}\left[\sum_{s',l'}T_{l'}(\alpha')\right]^{J}}{\left[\sum_{\alpha'',s'',l''}T_{l''}(\alpha'')\right]^{J}}Z(lJlJ,SL)Z(l'Jl'J,S'L)(-1)^{S-S'}P_{L}(\cos\theta), \tag{1}$$

where α and α' specify incident and exit channels, respectively, I and i are intrinsic spins of the target and projectile, and J denotes the compound nuclear spin. l is the orbital angular momentum and S is the channel spin in the entrance channel. The primed symbols denote corresponding quantities in the exit channel. T_{l}'s are the optical model transmission coefficients calculated using a computer program. The optical model and level density parameters for the channels used in the present calculations are listed in Tables I and II, respectively. The sum in the denominator of Eq. (1) extends over all discrete and continuum states. The level density prescriptions of Refs. [25,26] were used for the continuum states while the data on discrete states were taken from existing compilations [27]. A computer code HAFEST [28] was used for calculating the average compound nuclear cross sections. The calculated differential cross sections at different

TABLE I. Optical model parameters for Hauser-Feshbach calculations.

Channel	V_{real} (MeV)	r_r (fm)	a_r (fm)	W (MeV)	r_w (fm)	a_w (fm)	r_c (fm)	Ref.
$^{12}C+^{12}C$	14.0	1.35	0.35	$0.4+0.1E_{c.m.}$	1.4	0.35	1.35	[21]
$^{10}B+^{14}N$	$7.5 + 0.4E_{c.m.}$	1.35	0.45	$0.4+0.125E_{c.m.}$	1.35	0.45	1.35	[22]
$^{8}Be+^{16}O$	14.0	1.35	0.49	$0.4+0.15E_{c.m.}$	1.35	0.49	1.35	[23]
$^{7}Li+^{17}F$	35.4	1.07	1.05	11.5	1.26	0.62	1.35	[24]
$^{6}Li+^{18}F$	35.5	1.42	0.92	7.94	1.71	0.89	1.35	[24]
$^{5}Li+^{19}F$	$7.5+0.4E_{c.m.}$	1.35	0.65	$0.4+0.125E_{c.m.}$	1.35	0.65	1.35	[22]
$\alpha+^{20}Ne$	50.0	1.15	0.59	2.0	1.15	0.46	1.35	[22]
$^{3}He+^{21}Ne$	155.0	0.71	0.8	15.0	1.17	0.6	0.92	[23]
$t+^{21}Na$	155.0	0.71	0.8	15.0	1.17	0.6	0.92	[23]
$d+^{22}Na$	117.0	1.05	0.86	18.9	1.09	0.54	1.3	[23]
$p+^{23}Na$	$56.0-0.55E_{c.m.}$	1.25	0.65	13.5[a]	1.25	0.47	1.25	[22]
$n+^{23}Mg$	$48.2-0.3E_{c.m.}$	1.25	0.65	11.5[a]	1.25	0.47	1.25	[22]

[a]Surface form factor only.

beam energies for the $^{12}C(^{12}C, \alpha)\,^{20}Ne^*$ reaction at $\theta_{lab}=8°$ and 12° are shown in Figs. 3 and 4, respectively, for various excited states of ^{20}Ne. The Hauser-Feshbach cross sections are shown only for those excited states of ^{20}Ne which are found to show isolated peaks as inferred from the widths of the peaks. The spin assignments are taken from the literature [27].

We observe from Figs. 3 and 4 that the Hauser-Feshbach calculations reproduce the average behavior of the cross section for the low-lying 0^+, 2^+, and 4^+ members of the ground state band, for both 8° and 12° data. However, these calculations fail to reproduce the average behavior of the cross section for the other excited states in ^{20}Ne, particularly, for the members of $8p$-$4h$ band starting at 7.19 MeV (7.19 MeV, 0^+; 7.83 MeV, 2^+; 9.04 MeV, 4^+; 12.14 MeV, 6^+; 15.87 MeV, 8^+) and also for the states at 13.93 MeV, 6^+ and 20.48 MeV, 8^+. It is also clear from Figs. 3 and 4 that in the energy range $E_{c.m.}$=24–38 MeV the observed prominent structures in the excitation functions have considerably larger cross sections than those expected from the statistical compound nuclear contributions.

The calculated differential cross sections for the $^{12}C(^{12}C,\,^{8}Be)\,^{16}O^*$ reaction at 12° and 0° leading to various excited states of ^{16}O are shown in Figs. 5 and 7, respectively, for different beam energies. The optical model parameters used in these calculations are listed in Table I. For the ''18 MeV'' broad peak the contributions from 17.15 MeV, 2^+; 18.05 MeV, 4^+; and 19.35 MeV, 6^+ excited states of ^{16}O are included in the Hauser-Feshbach calculations. We observe from Figs. 5 and 7 that the Hauser-Feshbach calculations reproduce the average behavior of the cross sections for ground state of ^{16}O only above $E_{c.m.}$=29 MeV. In fact the prominent structures in the excitation functions have considerably larger cross sections than the calculated ones.

B. Statistical fluctuations versus nonstatistical structures

In the present work, the excitation energy of ^{24}Mg ranges from 38 to 53 MeV. From the known level densities in this region of excitation overlapping levels leading to statistical fluctuations in the excitation functions are expected [17]. The presence of any nonstatistical structure in the excitation functions can be identified by the cross correlation among various channels. Another method is to sum the excitation functions leading to different excited states so that the statistical fluctuations are smeared out, leaving only the nonstatistical resonant structures.

Figure 10(a) shows such an excitation function for the reaction $^{12}C(^{12}C, \alpha)\,^{20}Ne$ averaged over both the angles and summed over all the channels leading to different excited states of ^{20}Ne. The average over angles included the proper angular weight factors. Figure 10(b) shows a similar excitation function for $^{12}C(^{12}C,\,^{8}Be)\,^{16}O$ averaging over the angles 12° and 0°, and summing over the excitation energies of 0.0, 6.13, 6.92/7.13, 10.35, 11.04, and 18.0 MeV in ^{16}O. A striking feature that emerges from Figs. 10(a) and 10(b) is that the there are two broad structures in both α and ^{8}Be excitation functions at $E_{c.m.}$=24–29 MeV (E_x=38–43 MeV) and $E_{c.m.}$=30–35 MeV (E_x=44–49 MeV). These broad peaks represent nonstatistical resonant structures since the statistical fluctuations would have been smeared out when so many channels were summed.

The excited states of ^{20}Ne have been studied in detail and there are several well-known alpha cluster bands identified in

TABLE II. Level density parameters for Hauser-Feshbach calculations.

Nucleus	^{12}C	^{14}N	^{16}O	^{17}F	^{18}F	^{19}F	^{20}Ne	^{21}Ne	^{21}Na	^{22}Na	^{23}Na	^{23}Mg	Ref.
a/A	0.149	0.152	0.149	0.152	0.152	0.152	0.165	0.19	0.19	0.177	0.184	0.166	[25]
Δ	5.13	0.0	5.13	2.67	0.0	2.67	5.13	2.44	2.67	0.0	2.67	2.46	[26]
E_{cut}	12.44	12.59	18.0	14.8	11.22	11.07	24.4	5.43	6.09	5.10	7.13	5.98	

[a]E_{cut} is energy in MeV up to which discrete levels were used in the calculation of the denominator in Eq. (1).

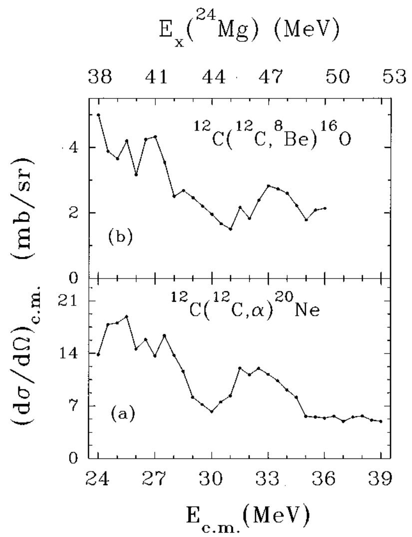

FIG. 10. (a) Summed excitation function for the $^{12}C(^{12}C,\alpha)$ ^{20}Ne reaction. Data at angles $\theta_{lab}=8°$ and 12° are averaged and summed over all 16 channels leading to different excited states of ^{20}Ne. (b) Summed excitation function for the $^{12}C(^{12}C,^{8}Be)^{16}O$ reaction. Data at 12° and 0° are averaged and summed for six different channels (0.0, 6.13, 6.92/7.13, 10.35, 11.04, and 18.0 MeV) in ^{16}O.

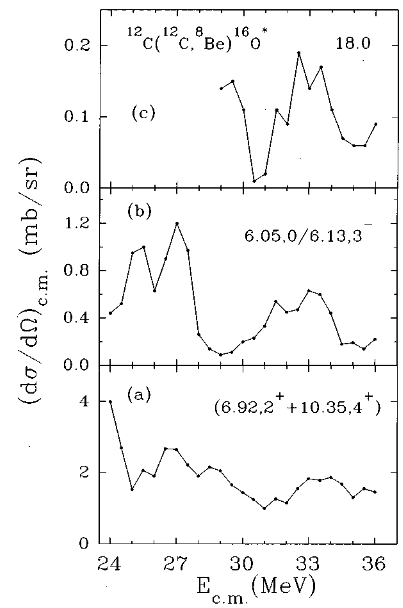

FIG. 12. (a) Excitation function for the $^{12}C(^{12}C,^{8}Be)^{16}O$ reaction averaged over the angles $\theta_{lab}=12°$ and 0° and (a) summed over 6.92 MeV, 2^+ and 10.35 MeV, 4^+ states of ^{16}O which are members of $4p$-$4h$ band, (b) for 6.05/6.13 MeV states of ^{16}O, and (c) leading to the ''18 MeV'' region of ^{16}O.

the spectrum [29]. The levels at 7.19 MeV, 0^+; 7.83 MeV, 2^+; 9.04 MeV, 4^+; 12.14 MeV, 6^+; and 15.87 MeV, 8^+ are classified as members of a $8p$-$4h$ triaxial band with ^{12}C + ^{8}Be cluster structure [29,30] while the 6.72, 0^+; 7.42, 2^+; 10.0, 4^+ and 13.93 MeV, 6^+ states are classified as a possible band with $^{16}O+\alpha$ cluster structure [29] with the 20.48 MeV level assigned tentatively as the 8^+ member of this band. The excitation functions of the $^{12}C(^{12}C,\alpha)$ ^{20}Ne reaction, averaged over both angles were, therefore, separated into two groups of final states. Figure 11(a) shows the excitation function leading to the 20.48 MeV, 8^+ state (not resolved from adjacent 20.7 MeV state), and Fig. 11(b) shows the summed excitation function leading to members of the $8p$-$4h$ triaxial band. An interesting feature that emerges from this separation is that the region of excitation in ^{24}Mg at E_x=39–43 MeV ($E_{c.m.}$ = 24–29 MeV) predominantly decays to the $8p$-$4h$ triaxial band in ^{20}Ne [Fig. 11(b)] and the region E_x=44–49 MeV ($E_{c.m.}$=30–35 MeV) decays predominantly to the 20.48 MeV, 8^+ state [Fig. 11(a)].

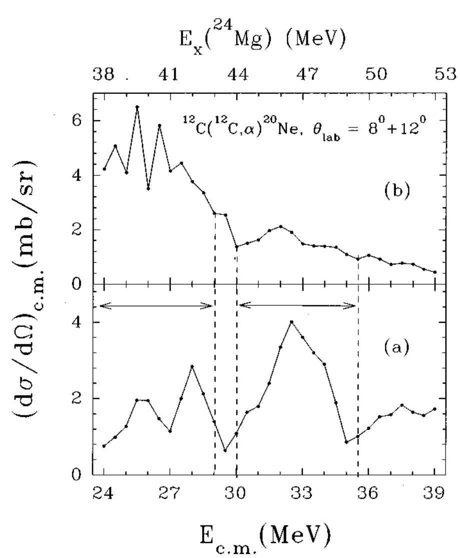

FIG. 11. (a) Excitation function for the $^{12}C(^{12}C,\alpha)$ ^{20}Ne reaction averaged over angles $\theta_{lab}=8°$ and 12° leading to (a) 20.48 MeV state of ^{20}Ne and (b) summed over five states (7.19, 7.84, 9.04, 12.14, and 15.87 MeV which are members of $8p$-$4h$ band) in ^{20}Ne.

In the case of ^{16}O there are excited states at 6.05 MeV, 0^+; 6.92 MeV, 2^+; and 10.35 MeV, 4^+ which are members of a $4p$-$4h$ rotational band. The 3^- octupole state occurs at 6.13 MeV. There are also levels at 17.15, 18.05, and 19.35 MeV with spins 2^+, 4^+, and 6^+, respectively, which decay into two ^{8}Be nuclei. These qualify to be the members of a rotational band with a large moment of inertia, consistent with that of a 4α linear chain [6]. The excitation function of the $^{12}C(^{12}C,^{8}Be)^{16}O$ reaction, averaged over 0° and 12° data, and summed over the final excited states of 6.92 MeV, 2^+ and 10.35 MeV, 4^+ ($4p$-$4h$ states) in ^{16}O, is shown in Fig. 12(a). Figure 12(b) shows the excitation function leading to the 6.13 MeV, 3^- state in ^{16}O and averaged over both the angles. The peak corresponding to the 6.13 MeV state can also contain the yield leading to 6.05 MeV, 0^+ state. However, this is found to be a small fraction from the ^{8}Be-γ coincidence measurement made in this work and discussed in the next section. Figure 12(c) shows the excitation function leading to the 18 MeV region of ^{16}O which includes the possible 4α linear chain band. Figure 12(a) shows a predominant broad peak in the region $E_{c.m.}$=25–30 MeV and a lower yield in the $E_{c.m.}$=30–35 MeV region. This is similar to the situation in $^{12}C(^{12}C,\alpha)$ ^{20}Ne where the lower region of $E_{c.m.}$=25–29 MeV decays to the $8p$-$4h$ band in ^{20}Ne [Fig. 11(b)]. It is clear from Fig. 12(b) that the 6.13 MeV, 3^- state of ^{16}O is fed both from the $E_{c.m.}$=24–28 MeV and 30–35

MeV regions. Figure 12(c) shows a broad peak in the $E_{\mathrm{c.m.}}$=30–35 MeV region corresponding to decay to the possible 4α-linear-chain states of ^{16}O. It is important to note that this broad peak is observed at both 12° and 0° measured with two completely different detector setups for ^{8}Be in two independent experiments. This broad structure is similar to the one observed in ^{12}C(^{12}C,α)^{20}Ne leading to the 20.48 MeV state of ^{20}Ne [Fig. 11(a)].

C. ^{8}Be-γ coincidence measurements in ^{12}C(^{12}C,^{8}Be)^{16}O$^{*}\rightarrow\gamma+^{16}O_{\mathrm{g.s.}}$

The excitation region near 6–7 MeV in ^{16}O includes states at 6.05 MeV, 0^{+}; 6.13 MeV, 3^{-}; 6.92 MeV, 2^{+}; and 7.13 MeV, 1^{-}. In the ^{8}Be energy spectrum (Figs. 2 and 6) there are two close peaks, one corresponding to the unresolved 6.05 MeV and 6.13 MeV states and the other corresponding to the 6.92 MeV and 7.13 MeV states. Since the 6.05 MeV, 0^{+} state is a $4p$-$4h$ state and 6.13 MeV, 3^{-} is an octupole state, it is of interest to know which of them is excited in the excitation function of ^{12}C(^{12}C,^{8}Be)^{16}O. The 6.05 MeV state cannot decay by one photon emission while the 6.13 MeV, 3^{-} state decays by octupole gamma radiation to the ground state of ^{16}O. This difference in their decay modes was used to quantify their relative excitation probabilities by a ^{8}Be-γ coincidence measurement. The coincidence excitation functions for ^{8}Be leading to 6.13 MeV, 3^{-} and 6.92 MeV, 2^{+}/7.13 MeV, 1^{-} states of ^{16}O are shown in Figs. 9(a) and 9(b), respectively.

The angular correlation function $W(\theta)$ for the γ-ray transition between two states with spin a and b is given by [31]

$$W(\theta)=\sum_{k}\left[\sum_{m}\rho_{k}(a,m)P(m)\right]F_{k}(a,b)Q_{k}P_{k}(\cos\theta), \tag{2}$$

where θ is the angle between the direction of the emission of the γ ray and the axis of alignment which is taken as the beam direction, $P_k(\cos\theta)$ are the Legendre polynomials, k takes only even values from 0 to $2a$, and Q_k are the attenuation coefficients due to the finite size of the γ-ray detector. The $\rho_k(a)$ are the statistical tensors describing the alignment of the initial state and are given by the weighted sum over the population parameter $P(m)$ of the magnetic substates of a. The coefficient $F_k(a,b)$ depends on the γ-ray multipolarities and generally only the two lowest multipolarities are included. The coefficients ρ_k and F_k are obtained from the tabulation of Poletti and Warburton [31] and Q_k are calculated by the expression given in Ref. [32]. Because ^{8}Be is detected at 0°, the population $P(m)$ is limited [33] to the $m=0$ substate in ^{16}O. The theoretical value of the ratio $R=W(138°)/W(90°)$ for the decay of the 6.13 MeV, 3^{-} state of ^{16}O to the ground state is 1.54 for our detector geometry. The average experimental value of this ratio is equal to 1.62 ± 0.17 which agrees with the theoretical value. The experimental value of R for the 6.92 MeV, 2^{+}/7.13 MeV, 1^{-} states of ^{16}O varies from 1 to 4 with beam energy. The theoretical value of this ratio for pure quadrupole (2^{+}) transition is 17.0 while for a pure dipole transition the value is 0.5. Since the experimental values of this ratio are near neither of the theoretical values, this indicates that the 6.92/7.13 MeV ^{8}Be peak includes the yields due to both these states with relative yields varying with beam energy. In order to estimate the contribution of the 6.13 MeV state of ^{16}O in the unresolved singles spectrum, we have calculated the angle-integrated 6.13-MeV γ-ray yield using the coincidence counts in the γ-ray detectors after correcting for the intrinsic efficiency and peak-to-total ratio of the detector. This calculation showed that the relative yield to the 6.13 MeV state varies between 75% and 90% over the beam energies spanning the $E_{\mathrm{c.m.}}$=32.5 MeV resonance.

TABLE III. Comparison of angle and $E_{\mathrm{c.m.}}$ averaged cross sections, X (see text) in the ^{12}C(^{12}C,α)^{20}Ne reaction leading to different 6^{+} and 8^{+} states in ^{20}Ne.

E_x(^{20}Ne) MeV	J^{π}	X (mb/sr)
12.14	6^{+}	0.239 ± 0.003
12.59	6^{+}	0.187 ± 0.003
13.93	6^{+}	0.323 ± 0.004
15.87	8^{+}	0.742 ± 0.005
18.54	8^{+}	1.308 ± 0.008
20.48	8^{+}	2.431 ± 0.011

IV. RESULTS AND DISCUSSION

The following points emerge from the analysis of the data in the previous section.

(1) ^{24}Mg in the excitation region of 38–43 MeV ($E_{\mathrm{c.m.}}$= 24–29 MeV) decays by α emission predominantly to the $8p$-$4h$ triaxial band in ^{20}Ne (7.19 MeV, 0^{+}; 7.83 MeV, 2^{+}; 9.04 MeV, 4^{+}; 12.14 MeV, 6^{+}; and 15.87 MeV, 8^{+} levels) and by ^{8}Be emission to the $4p$-$4h$ band in ^{16}O (6.92 MeV, 2^{+}; 10.35 MeV, 4^{+} levels)

(2) ^{24}Mg in the excitation region of 44–49 MeV (centered at $E_{\mathrm{c.m.}}$=32.5 MeV) decays predominantly by α emission to 20.48 MeV state in ^{20}Ne and also by ^{8}Be emission to the 18 MeV region in ^{16}O where the 4α-linear-chain band is possibly located [6].

The measured cross sections in the ^{12}C(^{12}C,α)^{20}Ne reaction were averaged over the angles θ_{lab}=8° and 12° and over $E_{\mathrm{c.m.}}$=30–35 MeV (E_x=44–49 MeV). Table III shows these cross sections for decay to the three 6^{+} states at 12.14, 12.59, and 13.93 MeV and to the three 8^{+} states at 15.87, 18.54, and 20.48 MeV in ^{20}Ne, in the last column, where X is defined as

$$X=\frac{\int\frac{d\sigma}{d\Omega}dE_{\mathrm{c.m.}}}{\int dE_{\mathrm{c.m.}}}. \tag{3}$$

In the above equation, the differential cross section is angle averaged. From Table III, it is clear that the 20.48 MeV, 8^{+} state is predominantly fed from the broad resonance region since the penetrabilities involved in all the cases have similar values (within 15%) as calculated using the optical model parameters given in Table I. ^{24}Mg in the above excitation region also decays by ^{8}Be emission to the 18 MeV region in

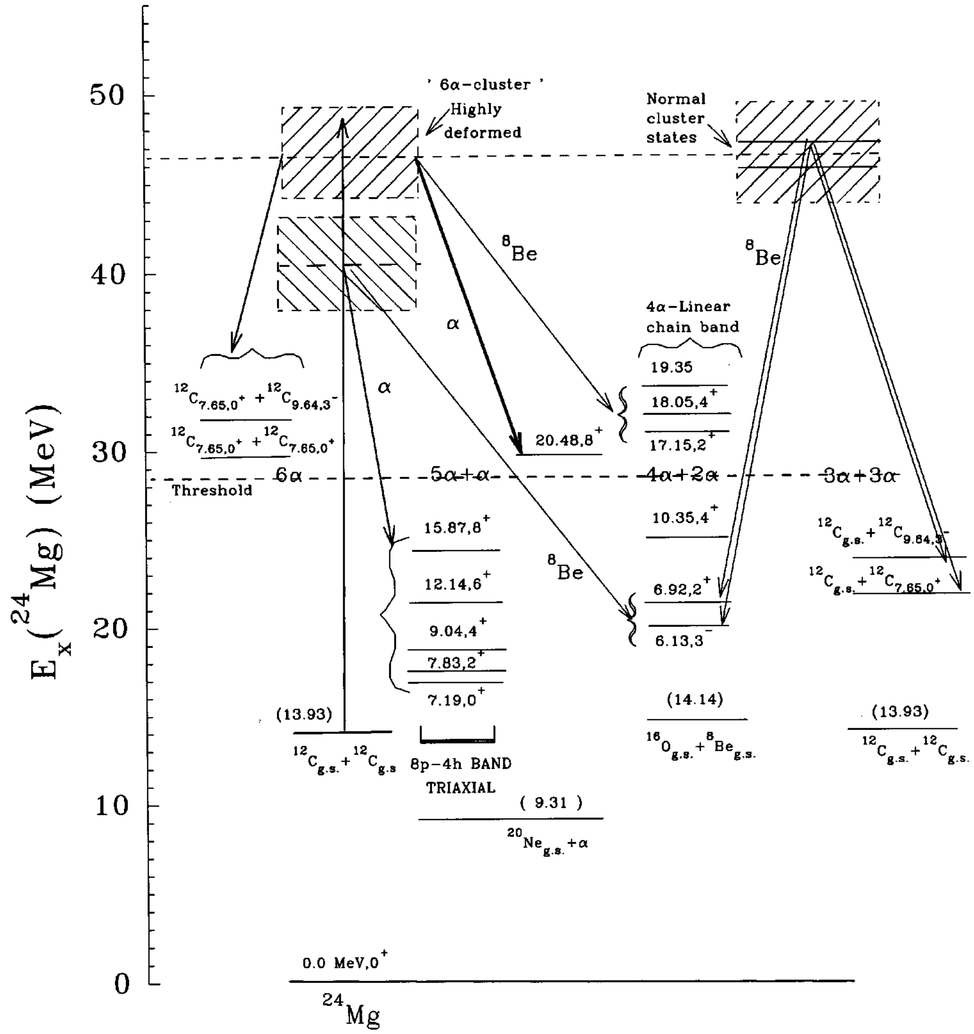

FIG. 13. Energy level diagram showing the decay modes of 6α-cluster resonance in ^{24}Mg at 46.4 MeV excitation. α and ^{8}Be decay modes shown are from the present work while decay in channels $^{12}C(0_2^+)+{}^{12}C(0_2^+)$ is from Wuosmaa *et al.* [7], in $^{12}C(0_2^+)+{}^{12}C(3^-)$ from Chappell *et al.* [8] and in $^{12}C_{g.s.}+{}^{12}C(0_2^+)$ and $^{12}C_{g.s.}+{}^{12}C(3^-)$ from Szilner *et al.* [36]. The dashed line indicates the breakup threshold for 6α, 5α, and 4α in ^{24}Mg, ^{20}Ne, and ^{16}O, respectively. Note that the highly deformed ''6α-cluster states'' in ^{24}Mg centered at E_x=46.4 MeV decay to final states above 6α breakup threshold. Normal cluster states at the same excitation energy decay to final states below the 6α breakup threshold.

^{16}O which includes the possible 4α-linear-chain band. It is significant to note that the 20.48 MeV state of ^{20}Ne and the 18 MeV region of ^{16}O are above the 5α and 4α breakup thresholds at 19.17 and 14.44 MeV, respectively. The 20.48 MeV, 8^+, state of ^{20}Ne is found to have decay branches of 66$\pm$ 26% to $^{16}O_{g.s.}+\alpha$, 14 $\pm$7% to $^{16}O^*+\alpha_{1+2}$, and 13 $\pm$2.5% to $^{12}C_{g.s.}+{}^{8}Be_{g.s.}$ as determined by Hindi *et al.* [29], indicating that it has a predominant α-cluster structure. The excitation energy region of ^{24}Mg centered at E_x=46.4 MeV was conjectured to have a 6α-cluster structure based on the experiments of Wuosmaa *et al.* [7,9]. In these experiments a strong resonance was observed at $E_{c.m.}$=32.5 MeV in the $^{12}C(^{12}C,{}^{12}C(7.65,0^+))^{12}C(7.65,0^+)$ reaction. This was confirmed by Chappell *et al.* [8] who observed the resonance in the above reaction as well as in the $^{12}C(^{12}C,{}^{12}C(7.65,0^+))^{12}C(9.64,3^-)$ reaction. In these reactions both the ^{12}C in the exit channel are above the 3α breakup threshold which is at 7.28 MeV in ^{12}C. Although there is a controversy as to whether this resonance at $E_{c.m.}$=32.5 MeV is the 6α-linear-chain state [8,10,11], the available data suggest that this resonance has a highly deformed 6α-cluster structure. It may be worth noting that the preferential decay of this structure to the 20.48 MeV state in ^{20}Ne, as seen in the present work, is indicative of the 5α-cluster structure of the 20.48 MeV state in ^{20}Ne. This conjecture is consistent with the hypothesis of Ikeda *et al.* [34] that multicluster structures appear at energies above the appropriate breakup thresholds. It is also consistent with the scenario that the highly deformed 6α-cluster resonance would tend to decay predominantly to a deformed 5α-cluster structure.

The preferential decay modes of ^{24}Mg in the excitation energy region of 38–50 MeV in the α and ^{8}Be channels, as identified in the present work, are pictorially represented in the energy level diagram shown in Fig. 13. Also shown in this diagram are the decay modes in the various inelastic channels studied by Wuosmaa *et al.* [7] and Chappell *et al.* [8]. The breakup thresholds for 6α, 5α, and 4α in ^{24}Mg, ^{20}Ne, and ^{16}O at 28.48 MeV, 19.17 MeV, and 14.44 MeV, respectively, are also shown in the figure.

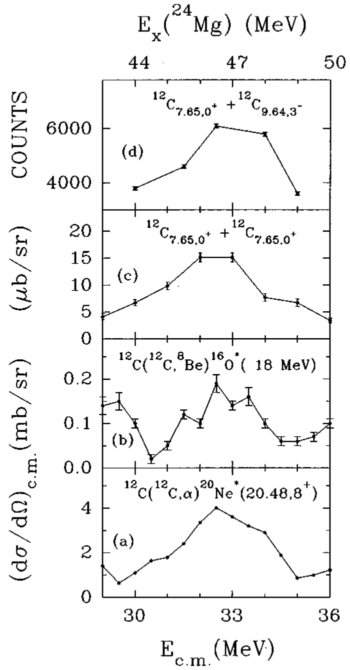

FIG. 14. Comparison of excitation functions for α, ^{8}Be, and inelastic scattering channels leading to states above 6α breakup threshold in ^{24}Mg. (a) $^{12}C(^{12}C,\alpha)^{20}Ne^{*}(20.48\ \mathrm{MeV},8^{+})$, (b) $^{12}C(^{12}C,^{8}Be)^{16}O^{*}(18.0\ \mathrm{MeV})$, (c) $^{12}C(^{12}C,^{12}C(0_2^+))^{12}C(0_2^+)$, and (d) $^{12}C(^{12}C,^{12}C(0_2^+))^{12}C(3^-)$. (a) and (b) are from present work and (c) and (d) are from Refs. [7] and [8], respectively.

Figure 14 shows the comparison of the excitation function in the region of 6α-cluster resonance centered at $E_{c.m.}=32.5$ MeV in four different channels. Figures 14(a) and 14(b) show the excitation function for $^{12}C(^{12}C,\alpha)^{20}Ne^{*}_{20.48,8^+}$ and $^{12}C(^{12}C,^{8}Be)^{16}O^{*}_{18.0}$, respectively, from the present work. Figure 14(c) shows that for $^{12}C(^{12}C,^{12}C_{7.65,0^+})^{12}C_{7.65,0^+}$ from Wuosmaa *et al.* [7] and Fig. 14(d) shows that for $^{12}C(^{12}C,^{12}C^{*}_{7.65,0^+})^{12}C^{*}_{9.64,3^-}$ from Chappell *et al.* [8]. All the above four cases are those where all the exit channels are above 5α, 4α, and 3α breakup thresholds in ^{20}Ne, ^{16}O, and ^{12}C, respectively, and also above the 6α breakup threshold in ^{24}Mg. The energy and width of the broad resonance in all these cases are observed to be similar. In particular, the excitation function for $^{12}C(^{12}C,\alpha)^{20}Ne^{*}(20.48)$ [Fig. 14(a)], in which the peak cross section is as much as 4 mb/sr, has a striking resemblance to the 6α-cluster resonance seen in $^{12}C(^{12}C,^{12}C(7.65,0^{+}))^{12}C(7.65,0^{+})$ [Fig. 14(c)]. The observations of decay modes shown in Figs. 14(a) and 14(b) give support to the conjecture of highly deformed 6α structure at the 46.4 MeV excitation region of ^{24}Mg with a large width of about 3–4 MeV. However, no definite statement can be made about the extent of deformation or about the linear nature of the 6α structure. If the deformation is as large as that for a 6α-linear-chain state, the coherent superposition of near-degenerate resonances with different spins would give rise to a large width as experimentally observed [10].

In the $^{12}C(^{12}C,^{8}Be)^{16}O^{*}_{6.13,3^-}$ reaction two intermediate resonance structures were observed at $E_{c.m.}=31.5$ and 33.5 MeV as well as at 25.0 and 27.0 MeV [Figs. 9(a) and 12(b)]. The resonances at $E_{c.m.}=31.5$ and 33.5 MeV are in the same energy region as the $E_{c.m.}=32.5$ MeV highly deformed 6 α-cluster resonance discussed earlier, but have smaller widths. However, these resonances are likely to have a different structure than that of the highly deformed 6α-cluster resonance which decays to states above the 6α breakup threshold. Strong resonances have also been observed in the inelastic scattering channels $^{12}C(^{12}C,^{12}C)^{12}C^{*}_{9.64,3^-}$ at $E_{c.m.}=33.5$ MeV with $J^{\pi}=18^{+}$ [9,35]. More recently it is reported by Szilner *et al.* [36] that in the inelastic channels $^{12}C_{g.s.}+{}^{12}C^{*}_{7.65,0^+}$, $^{12}C_{g.s.}+{}^{12}C^{*}_{9.64,3^-}$, and $^{12}C_{g.s.}+{}^{12}C^{*}_{14.08,4^+}$, correlated intermediate width structures were observed at $E_{c.m.}=31.0$, 32.5, and 33.5 MeV whose widths are appreciably smaller than those measured in the $^{12}C_{7.65,0^+}+{}^{12}C_{7.65,0^+}$ channel [7]. It is likely that the structures seen at $E_{c.m.}=31.5$ and 33.5 MeV in the $^{8}Be_{g.s.}+{}^{16}O^{*}_{6.13,3^-}$ channel in our work are the same as those seen in the $^{12}C_{g.s.}+{}^{12}C^{*}_{9.64,3^-}$ channel reported in Refs. [9,36].

Recently another work has been reported by Le Marechal *et al.* [37] on the investigation of the $^{12}C+{}^{12}C$, $E_{c.m.}=32.5$ MeV resonance with fine step excitation function measurements. They observe correlated structure in the inelastic scattering exit channels involving 0_2^+ and 3^- states of ^{12}C and in the $^{16}O_{g.s.}+{}^{8}Be$ channel with different widths.

In conclusion, it is conjectured that in the excitation region $E_x=44$–49 MeV centered at $E_{c.m.}=32.5$ MeV in $^{12}C+{}^{12}C$ collisions two types of states are excited. One type has a highly deformed 6α-cluster structure, leading to final states in which both the products are above the threshold for break up into constituents alpha particles. The other type of states are not so highly deformed and decay to final states which are below the 6α breakup threshold in ^{24}Mg. These two types of states are indicated in the left and right sides of the Fig. 13, respectively.

ACKNOWLEDGMENTS

We highly appreciate the cooperation of the operating staff in the smooth and efficient running of the Pelletron accelerator. Our special thanks are also due to Dr. Srikantiah and his colleagues from Technical Physics and Prototype Engineering division of BARC for providing TWIN surface barrier detectors which are used in the present work for detection of ^{8}Be particles.

[1] E. Almqvist, D. A. Bromley, and J. A. Kuehner, Phys. Rev. Lett. **4**, 515 (1960); D. A. Bromley, J. A. Kuehner, and E. Almqvist, Phys. Rev. C **123**, 878 (1961).
[2] S. Marsh and W. D. M. Rae, Phys. Lett. B **180**, 185 (1986).
[3] G. Leander and S. E. Larsson, Nucl. Phys. **A239**, 93 (1975).
[4] H. Flocard P. H. Heenen, S. J. Kreiger, and M. S. Weiss, Prog. Theor. Phys. **72**, 1000 (1984).
[5] N. de Takacsy and S. Das Gupta, Phys. Lett. **33B**, 556 (1970);

H. Friedrich, L. Satpathy, and A. Weiguny, *ibid.* **36B**, 189 (1971); N. de Takacsy, Nucl. Phys. **A178**, 469 (1972); Chr. Bargholtz, *ibid.* **A243**, 449 (1975)

[6] M. Freer *et al.*, Phys. Rev. C **51**, 1682 (1995); P. Chevallier, F. Scheibling, G. Goldring, I. Plesser, and W. M. Sachs, Phys. Rev. **160**, 827 (1967).

[7] A. H. Wuosmaa, R. R. Betts, B. B. Back, M. Freer, B. G. Glagola, Th. Happ, D. J. Henderson, P. Wilt, and I. G. Bearden, Phys. Rev. Lett. **68**, 1295 (1992); Phys. Rev. C **50**, 2909 (1994).

[8] S. P. G. Chappell, D. L. Watson, S. P. Fox, C. D. Jones, W. D. M. Rae, P. M. Simmons, M. Freer, B. R. Fulton, N. M. Clarke, N. Curtis, M. J. Leddy, J. S. Pople, S. J. Hall, R. P. Ward, G. Tungate, W. N. Catford, G. J. Gyapong, S. M. Singer, and P. H. Regan, Phys. Rev. C **51**, 695 (1995).

[9] A. H. Wuosmaa, B. B. Back, R. R. Betts, M. Freer, B. G. Glagola, D. J. Henderson, D. J. Hofman, and V. Nanal, Phys. Rev. C **54**, 2463 (1996).

[10] W. D. M. Rae, A. C. Merchant, and B. Buck, Phys. Rev. Lett. **69**, 3709 (1992).

[11] W. D. M. Rae and A. C. Merchant, Phys. Rev. Lett. **74**, 4145 (1995).

[12] E. T. Mirgule, Suresh Kumar, M. A. Eswaran, D. R. Chakrabarty, V. M. Datar, N. L. Ragoowansi, H. H. Oza, and U. K. Pal, Nucl. Phys. **A583**, 287c (1995).

[13] G. J. Wozniak, N. A. Jelley, and Joseph Cerny, Nucl. Instrum. Methods **120**, 29 (1974).

[14] Suresh Kumar, M. A. Eswaran, and E. T. Mirgule, in Proceedings of the Nuclear Physics Symposium (DAE, Bombay, 1991), Vol. 34B, p. 427.

[15] G. J. Wozniak, H. L. Harney, K. H. Wilcox, and J. Cerny, Phys. Rev. Lett. **29**, 1278 (1972).

[16] M. L. Halbert, F. E. Durham, and A. Van der Woude, Phys. Rev. **162**, 899 (1967).

[17] L. C. Dennis, S. T. Thorton, and K. R. Cordell, Phys. Rev. C **19**, 777 (1979).

[18] D. B. Brink and R. O. Stephen, Phys. Rev. Lett. **5**, 77 (1963); T. E. O. Ericson and T. Mayer-Kuckuk, Annu. Rev. Nucl. Sci. **16**, 183 (1966).

[19] W. Hauser and H. Feshbach, Phys. Rev. **87**, 366 (1952).

[20] R. G. Stokstad, in *Treatise on Heavy Ion Science*, edited by D. A. Bromley (Plenum, New York, 1985), Vol. 3, p. 83.

[21] W. Reilley, R. Wieland, A. Gobbi, M. W. Sachs, J. Maher, R. H. Siemssen, D. Mingay, and D. A. Bromley, Nuovo Cimento A **13**, 897 (1973).

[22] L. R. Greenwood, R. E. Segel, K. Raghunathan, M. A. Lee, H. T. Fortune, and J. J. Erskine, Phys. Rev. C **12**, 156 (1975).

[23] D. Shapira, R. G. Stokstad, and D. A. Bromley, Phys. Rev. C **10**, 1063 (1964).

[24] K. Bethge, C. M. Fou, and R. W. Zurmuhle, Nucl. Phys. **A123**, 512 (1969).

[25] D. W. Lang, Nucl. Phys. **A42**, 353 (1963).

[26] A. Gilbert and A. G. W. Cameron, Can. J. Phys. **43**, 1446 (1965).

[27] F. Ajzenberg-Selove, Nucl. Phys. **A475**, 1 (1987).

[28] M. A. Eswaran, Suresh Kumar, E. T. Mirgule, and N. L. Ragoowansi, Phys. Rev. C **39**, 1856 (1989).

[29] M. M. Hindi, J. H. Thomas, D. C. Radford, and P. D. Parkar, Phys. Rev. C **27**, 2902 (1983).

[30] M. A. Eswaran, Suresh Kumar, E. T. Mirgule, D. R. Chakrabarty, V. M. Datar, U. K. Pal, and N. L. Ragoowansi, Phys. Rev. C **47**, 1418 (1993); R. J. Ledoux, C. E. Ordonez, M. J. Bechara, H. A. Al-Jumair, G. Larelle, and E. R. Cosman, Phys. Rev. C **30**, 866 (1984).

[31] A. R. Poletti and E. K. Warburton, Phys. Rev. **137**, B595 (1965).

[32] M. E. Rose, Phys. Rev. **91**, 610 (1953).

[33] A. E. Litherland and A. J. Ferguson, Can. J. Phys. **39**, 788 (1961).

[34] K. Ikeda, N. Takigawa, and H. Horiuchi, Prog. Theor. Phys. Suppl. Extra Number, 464 (1968).

[35] B. R. Fulton, T. M. Cormier, and B. J. Herman, Phys. Rev. C **21**, 198 (1980).

[36] S. Szilner, Z. Basrak, R. M. Freeman, F. Haas, A. Morsad, and C. Beck, Phys. Rev. C **55**, 1312 (1997).

[37] R. A. Le Marechal, N. M. Clarke, M. Freer, B. R. Fulton, S. J. Hall, S. J. Hoad, G. R. Kelly, R. P. Ward, C. D. Jones, P. Lee, and D. L. Watson, Phys. Rev. C **55**, 1881 (1997).